Structural and biochemical characterization of *Mycobacterium tuberculosis* CYP142: Evidence for multiple cholesterol 27-hydroxylase activities in a human pathogen

[1]Max D. Driscoll, [1]Kirsty J. McLean, [1]Colin Levy, [2]Natalia Mast, [2]Irina A. Pikuleva, [3]Pierre Lafite, [1]Stephen E. J. Rigby, [1]David Leys, and [1]Andrew W. Munro*

[1]Manchester Interdisciplinary Biocentre, Faculty of Life Sciences, University of Manchester, 131 Princess Street, Manchester M1 7DN, UK. [2]Department of Ophthalmology and Visual Sciences, Case Western Reserve University, Cleveland, Ohio, USA. [3]ICOA-UMR, CNRS 6005, Université d'Orléans, Rue de Chartres, 45067 Orléans, France.

Running title: Structure and function of *Mycobacterium tuberculosis* CYP142

*Address correspondence to: A. W. Munro Tel: +44 161 3065151; Fax: +44 161 3068918; E-mail: Andrew.Munro@Manchester.ac.uk

Supplemental Data

Supplemental Experimental Procedures

Determination of a CYP142 extinction coefficient

The determination of an extinction coefficient for CYP142 in its oxidized form was done using the method of Berry and Trumpower (1). UV-vis. absorbance spectra were recorded for a CYP142 solution (for both 5 and 10 μM enzyme) before and after the addition of an equal volume of a 40% pyridine solution containing 0.8 mM potassium ferricyanide and 200 mM NaOH. Further spectra were recorded after the addition of a few grains of sodium dithionite. The concentration of CYP142 was calculated using the difference in absorbance between the spectra for the oxidized and reduced samples, using a difference extinction coefficient of $\Delta\varepsilon_{555}$ = 23.98 mM^{-1} cm^{-1}.

Determination of the redox potential for the heme iron Fe^{3+}/Fe^{2+} couple of CYP142

5 mL of oxidized CYP142 (~10 μM) was prepared in 100 mM KPi, 10% glycerol pH 7.0 and reduced by the stepwise addition of sodium dithionite to a complete ferrous state. CYP142 was then reoxidized to the ferric form with potassium ferricyanide. Titrations were done for both the substrate-free CYP142 enzyme and for the cholest-4-en-3-one (20 μM) bound form. Mediators were added to expedite electrical communication between the protein sample and the electrode, as described previously (2). Spectra (250–800 nm) were recorded using a Cary UV-50 UV–visible scanning spectrophotometer and the electrochemical potential of the solution was measured using a Mettler Toledo SevenEasy meter coupled to a Pt/Calomel electrode

(ThermoRussell Ltd.) at 25 ± 2 °C. The electrode was calibrated using the Fe^{3+}/Fe^{2+} EDTA couple as a standard (108 mV). A factor of 244 mV was used to correct relative to the normal hydrogen electrode. Absorbance changes at the heme Soret maximum were plotted against the applied potential, and data were fitted to the Nernst equation to derive the midpoint potential for the CYP142 heme Fe^{3+}/Fe^{2+} transition. Data manipulation and analysis were performed using Origin software.

Supplemental Results

Determination of an extinction coefficient for Mtb CYP142 using the pyridine hemochromogen method

The extinction coefficient for CYP142 was determined using the pyridine hemochromogen method as described by Berry and Trumpower (1). Figure S1 shows spectral details for oxidized CYP142 along with the spectra for the oxidized pyridine hemochrome form after reaction with pyridine, and for the reduced pyridine hemochrome after reduction with sodium dithionite. The heme concentration was determined from the change in absorption at the maximum in the difference spectrum generated by subtraction of the oxidized hemochrome spectrum from that of the reduced hemochrome. The heme concentration was determined using $\Delta\varepsilon_{555}$ = 23.98 mM^{-1} cm^{-1}. This leads to the establishment of an absolute coefficient for the extensively low-spin (LS) substrate-free CYP142 of ε_{418} = 140 mM^{-1} cm^{-1}.

EPR spectroscopic analysis of the substrate-bound form of CYP142

The cholest-4-en-3-one bound form of CYP142 was found to retain a proportion of high-spin (HS) P450 heme iron at 10 K. Figure S2 shows overlaid spectra for the low-spin (LS) substrate-free CYP142 and for the cholest-4-en-3-one bound enzyme, which is extensively HS at ambient temperature. While both spectra are dominated by the LS ferric heme iron component with *g*-values at 2.40, 2.23 and 1.92, there is a smaller signal from the HS ferric heme component in the cholest-4-en-3-one bound enzyme with *g*-values at 7.87, 3.65 and 1.71.

Redox potentiometric analysis of substrate-free and cholest-4-en-3-one bound CYP142

Spectroelectrochemical analysis of CYP142 in its substrate-free and cholest-4-en-3-one bound forms was done as described in the *Experimental Procedures* section of the main paper (3-5). Figure S3 shows overlaid plots of % heme oxidized (from data at the Soret maximum) *versus* applied potential, with data fitted to the Nernst function to produce midpoint reduction potentials (*vs*. NHE) for the Fe^{3+}/Fe^{2+} couple of -416 ± 6 mV (substrate-free CYP142) and -192 ± 7 mV (cholest-4-en-3-one bound CYP142). The large change in potential at least in part reflects the substantial switch in ferric heme iron spin-state equilibrium from LS to HS that CYP142 exhibits on binding cholest-4-en-3-one. Figure S4 shows plots of heme absorption (at 393 nm, close to the Soret maximum for the ferric cholest-4-en-3-one bound CYP142) *versus* applied potential for three successive rounds of reductive (using sodium dithionite) and oxidative (using potassium ferricyanide) titrations for the cholest-4-en-3-one bound P450. Redox titrations were again done as described in the *Experimental Procedures* section in the main paper. The data indicate clearly

a hysteretical behavior in each of the reductive and oxidative passes, whereby the reductive titration sets consistently have a midpoint potential of ~ -195 mV *vs*. NHE (as determined also in Figure S3), whereas the oxidative titration sets consistently have a potential of ~ -295 mV *vs*. NHE.

Analysis of CYP142 oxidation products from cholesterol and cholest-4-en-3-one

Under similar conditions, CYP142 generates 27-hydroxycholesterol from cholesterol substrate using *E. coli* flavodoxin reductase and flavodoxin (FLDR/FLD) as redox partners, and 5-cholestenoic acid using spinach ferredoxin reductase and ferredoxin (spFDR/spFDX) as redox partners (see main paper text and Figure 6 in main paper). Figure S5 shows GC-MS analysis of the methyl ester-trimethylsilyl ether of authentic 5-cholestenoic acid (panel A) and of the trimethylsilyl ether of authentic 27-hydroxycholesterol (panel B). Characteristic ions with m/z = 373, 412 and 502 are observed in the 5-cholestenoic acid standard mass spectrum (Figure S5) and also in the MS analysis of the CYP142 products with the spFDR/spFDX redox partners (Figure 6, main paper). Characteristic ions with m/z = 417, 456 and 546 are observed in the 27-hydroxycholesterol standard mass spectrum (Figure S5) and also in the MS analysis of the CYP142 products with the *E. coli* FLDR/FLD redox partners (Figure 6, main paper). These data confirm production of either 27-hydroxycholesterol or 5-cholestenoic acid from cholesterol substrate by CYP142 according to the particular redox partner system used. Characteristic ions from 27-hydroxycholesterol or 5-cholestenoic acid were assigned as shown in Figure S6. Figure S7 shows results from HPLC separations of CYP142 reactions with cholest-4-en-3-one substrate as a substrate using UV detection at 241 nm. As for the reactions with cholesterol, CYP142 forms a single major product with the *E. coli* FLDR/FLD redox system with a retention time distinct from the single major product with the spinach spFDR/spFDX redox system. By comparison with the HPLC analysis for the respective products of cholesterol oxidation (Figure 6, main paper), the cholest-4-en-3-one products are assigned to 27-hydroxycholest-4-en-3-one (FLDR/FLD) and cholest-4-en-3-one-27-oic acid (spFDR/spFDX).

Assignment of polyethylene glycol as a ligand in the CYP142 active site

Following completion of the CYP142 model, additional density was clearly visible in the active that could not be accounted for by solvent atoms. This density appeared to correspond to a partially ordered PEG molecule derived from the mother liquor (which was supplemented with 10% PEG 200 upon cryo-cooling of the crystals). The PEG was modeled with the terminal alcohol group ligating to the heme iron (as visible from the continuous electron density). A final electron density map and associated model is shown in Figure S8.

Binding of cholesterol to CYP142

Binding of cholesterol to CYP142 was done as described in the *Experimental Procedures* section of the main paper, using 6.8 μM CYP142. Cholesterol bound to CYP142 to induce a low-spin to high-spin shift in the heme iron spin-state equilibrium, and with a clear spectral shift from 418 nm towards 393 nm. Due to limited solubility of the cholesterol, the extent of conversion to the high-spin form was not as extensive as that observed using cholest-4-en-3-one (see Figure 2

in main paper), and the titration did not go to completion with some reconversion of CYP142 spin-state towards low-spin observed at higher cholesterol concentrations and turbidity noted at >10 μM cholesterol. By fitting data in the range up to 5 μM cholesterol, a K_d value of 0.34 ± 0.20 μM was determined (similar to the value of 0.36 μM for cholest-4-en-3-one). However, the K_d for cholesterol could be even lower than this estimate. Spectral data from the CYP142 cholesterol titration are shown in Figure S9.

Supplementary References

1. Berry, E. A., and Trumpower, B. L. (1987) *Anal. Biochem.* **161**, 1-15.

2. McLean, K.J., Lafite, P., Levy, C., Cheesman, M.R., Mast, N., Pikuleva, I.A., Leys, D., and Munro, A.W. (2009) *J. Biol. Chem*. **284**, 35524-35533.

3. Daff, S. N., Chapman, S. K., Turner, K. L., Holt, R. A., Govindaraj, S., Poulos, T. L., and Munro, A. W. (1997) *Biochemistry* **36**, 13816-13823.

4. Girvan, H. M., Marshall, K. R., Lawson, R.J., Leys, D., Joyce, M.G., Clarkson, J., Smith, W.E., Cheesman, M.R., and Munro, A.W. (2004). *J. Biol. Chem*. **279,** 23274-23286.

5. Dutton, P.L. (1978) *Methods Enzymol*. **54**, 411-435.

Figure Legends

Figure S1. Pyridine hemochromogen for CYP142. Main panel shows spectra for oxidized, substrate-free CYP142 (4.4. μM, solid line), the oxidized pyridine hemochrome form following mixing with pyridine (dashed line), and the reduced pyridine hemochrome following reduction with sodium dithionite (dotted line). The inset shows detail from the 500-610 nm regions of these spectra. An absolute extinction coefficient of ε_{418} = 140 mM^{-1} cm^{-1} for oxidized, substrate-free CYP142 was determined from the difference between oxidized and reduced pyridine hemochrome spectra using $\Delta\varepsilon_{555}$ = 23.98 mM^{-1} cm^{-1} (1).

Figure S2. EPR spectrum for cholest-4-en-3-one bound CYP142. X-band EPR spectra are overlaid for the LS, substrate-free oxidized CYP142 (black spectrum) and for the cholest-4-en-3-one substrate-bound CYP142 (red spectrum). The substrate-bound CYP142 is extensively high-spin (HS) at room temperature. At 10 K, the EPR spectra for both forms of the enzyme show features at g_x = 2.40, g_y = 2.23 and g_z = 1.92, indicative of LS ferric heme iron. In the substrate-bound form there is a second, minor set of *g*-values at g_x = 7.87, g_y = 3.65 and g_z = 1.71 indicative of the retention of HS heme iron in a proportion of the cholest-4-en-3-one bound enzyme at 10 K.

Figure S3. Redox potentiometry analysis of substrate-free and cholest-4-en-3-one bound CYP142. UV-visible absorption spectra were collected at several different reduction potentials during redox titrations of CYP142 in both substrate-free and cholest-4-en-3-one bound forms, as described in *Experimental Procedures* in the main paper. Absorbance changes at 418 nm (substrate-free) and at 393 nm (cholest-4-en-3-one bound) were used to determine midpoint potentials for the two forms of the enzyme, and data were then normalized for % heme oxidized and overlaid (filled squares, cholest-4-en-3-one bound; filled circles, substrate-free). The midpoint redox potentials (*versus* NHE) for the CYP142 heme Fe^{3+}/Fe^{2+} couples are -416 ± 6 mV (substrate-free) and -192 ± 7 mV (cholest-4-en-3-one bound).

Figure S4. Hysteresis in reductive and oxidative phases of a redox titration of cholest-4-en-3-one bound CYP142. CYP142 (10 μM) in its substrate-bound form (cholest-4-en-3-one, 50 μM) was successively reduced (with dithionite) and reoxidized (with ferricyanide) as described in *Experimental Procedures* in the main paper. Between 6-8 points were collected in each reductive and oxidative phase of the titration. Points from reductive phases are shown as open circles, with points from oxidative phases show as filled circles. The midpoint potential for the reductive phases is at ~ -195 mV, whereas that for the oxidative phases is at ~ -295 mV in each case. The collected data for reductive and oxidative sets are both fitted using the Nernst function.

Figure S5. GC-MS analysis of standards for CYP142 cholesterol oxidation products. GC-MS data for cholesterol standards are shown. Panel A: Mass spectrum following GC separation of the methyl ester-trimethylsilyl ether derivative of 5-cholestenoic acid showing characteristic ions with m/z values at 373, 412 and 502 (molecular ion). Panel B: Mass spectrum following GC

separation of the trimethylsilyl ether derivative of 27-hydroxycholesterol showing characteristic ions with m/z values at 417, 456 and 546 (molecular ion).

Figure S6. **Chemical assignments of ions identified in the fragmentation patterns from GC-MS analysis of 27-hydroxycholesterol and 5-cholestenoic acid**. Chemical identities of fragments generated from the methyl ester-trimethylsilyl ether derivative of 5-cholestenoic acid (Panel A) and from the trimethylsilyl ether derivative of 27-hydroxycholesterol (Panel B), allowing assignment of the relevant oxidation products generated by spFDR/spFDX and *E. coli* FLDR/FLD, respectively (see Figure S5 and Figure 6 in main text of the paper).

Figure S7. HPLC separation of the extracts from the CYP142 incubations with cholest-4-en-3-one substrate. The HPLC profile with the spinach spFDR/spFDX redox system is shown with a solid line. A single dominant product with retention time 8.26 min is seen. The HPLC profile with the *E. coli* FLDR/FLD redox system is shown with a dashed line. A single dominant product with retention time 9.37 min is seen. By comparison with the cholesterol oxidation products using the same redox systems (Figure 6, main paper), we assign the products of 4-cholesten-3-one oxidation by CYP142 to cholest-4-en-3-one-27-oic acid (spFDR/spFDX) and 27-hydroxycholest-4-en-3-one (FLDR/FLD). The concentration of cholest-4-en-3-one was 1 μM and UV detection was at 241 nm.

Figure S8. CYP142 heme with partially ordered PEG200. The heme moiety and associated PEG molecule are shown in atom colored sticks. The corresponding electron density is contoured at 1 sigma and is shown in a blue mesh.

Figure S9. Binding of cholesterol to CYP142. The main panel shows UV-visible absorption spectra from a titration of cholesterol with CYP142 (6.8 μM). Spectra shown are in absence of cholesterol (black solid line), with 1 μM cholesterol (red solid line), 2 μM cholesterol (green solid line), 3 μM cholesterol (dark blue solid line), 4 μM cholesterol (light blue solid line), 5 μM cholesterol (magenta solid line) and 8 μM cholesterol (black dashed line). Some reconversion from high-spin towards low-spin heme is observed at higher concentrations of cholesterol, with notable turbidity above 10 μM cholesterol. Inset shows a fit of cholesterol induced absorption change (ΔA_{387} minus ΔA_{420}, reflecting peak and trough values in difference spectra computed by subtracting the spectrum for cholesterol-free CYP142 from each of the spectra for the cholesterol-bound forms) versus [cholesterol] added, with data fitted to equation 1 (see main text) to generate an apparent K_d value of 0.34 ± 0.20 μM for cholesterol binding to CYP142. The solid line indicates the data fit up to 5 μM cholesterol, with the dashed line indicating the projected fit beyond these points using equation 1.

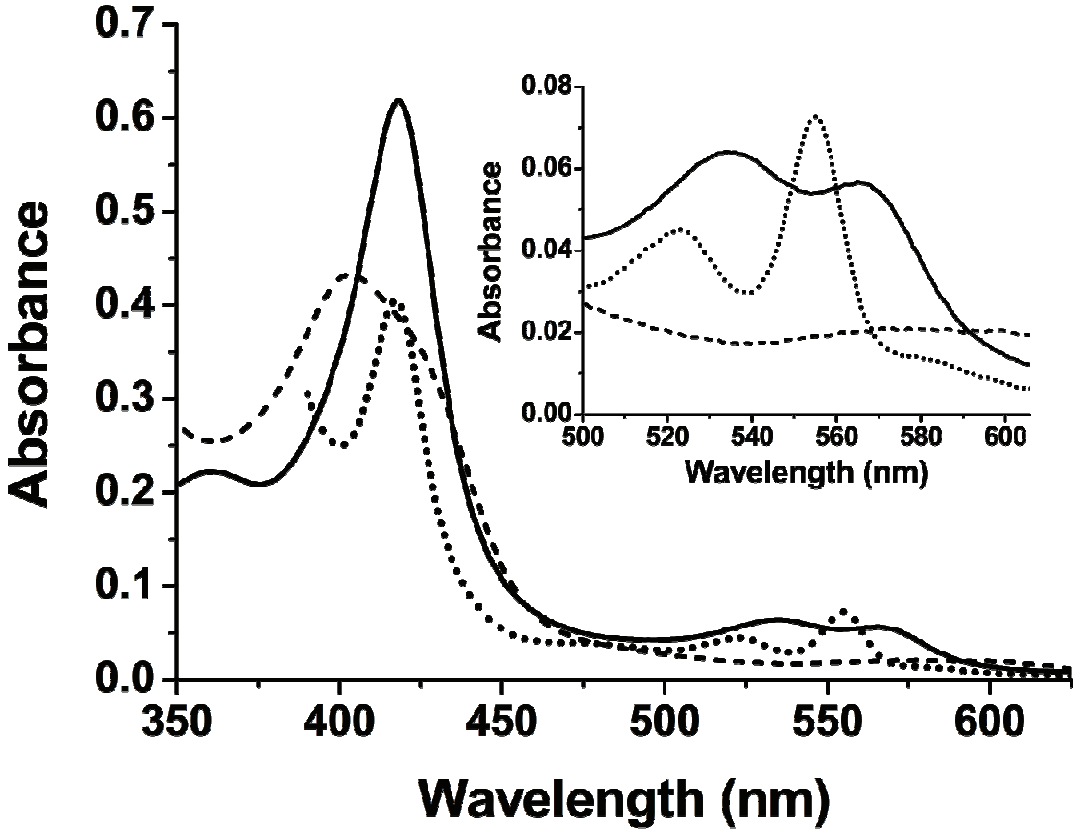
Absorbance
Wavelength (nm)
0.0
0.1
0.2
0.3
0.4
0.5
0.6
0.7
350
400
450
500
550
600
Absorbance
Wavelength (nm)
0.00
0.02
0.04
0.06
0.08
500
520
540
560
580
600

Figure S1

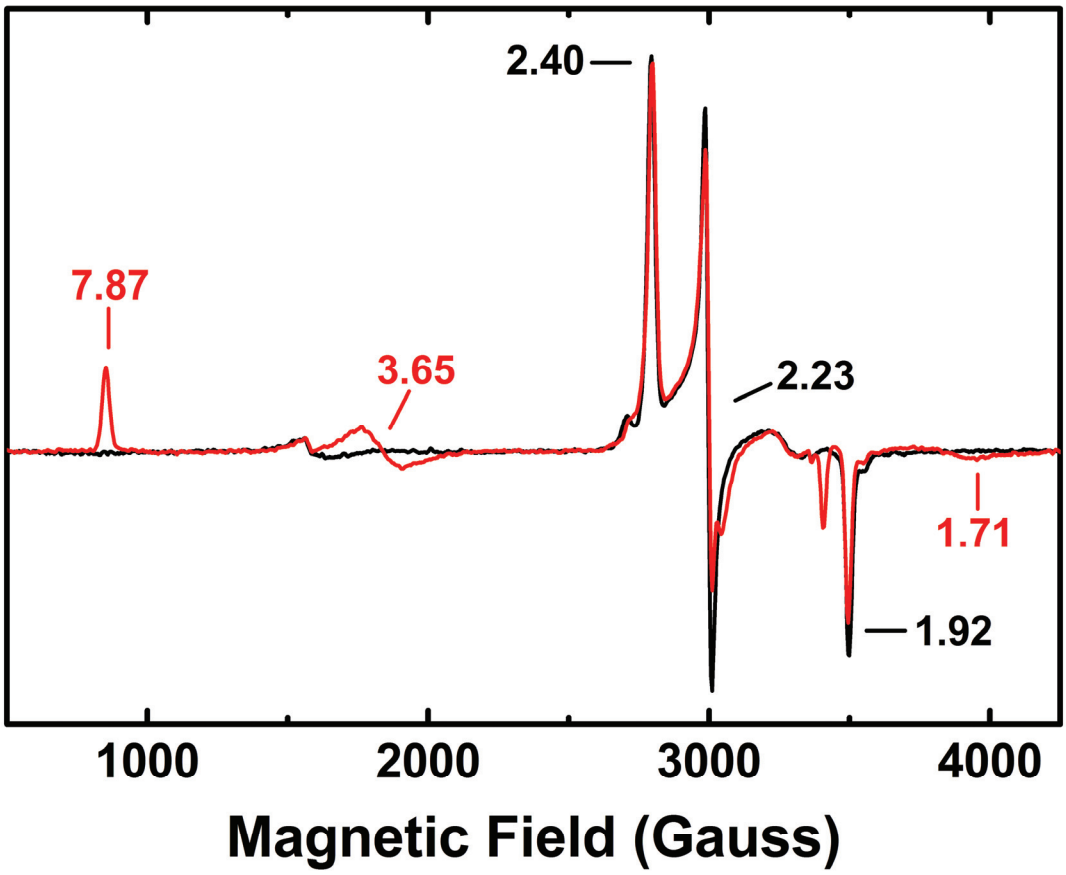
2.40
7.87
3.65
2.23
1.71
1.92
1000
2000
3000
4000
Magnetic Field (Gauss)

Figure S2

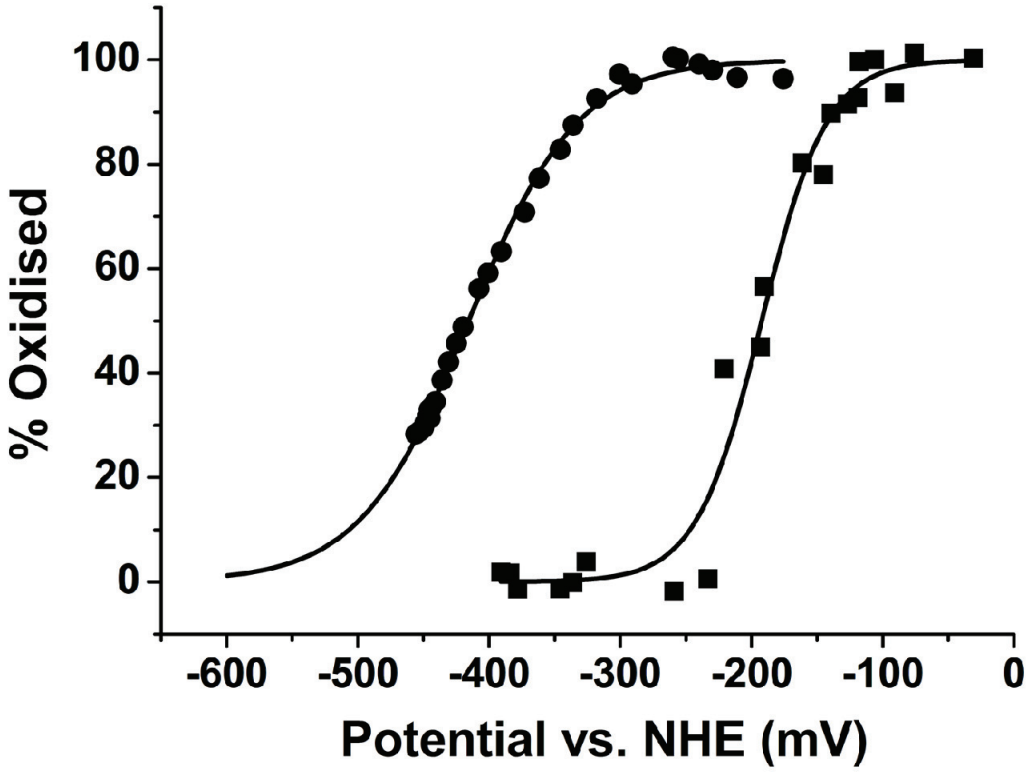
% Oxidised
100
80
60
40
20
0
-600
-500
-400
-300
-200
-100
0
Potential vs. NHE (mV)

Figure S3

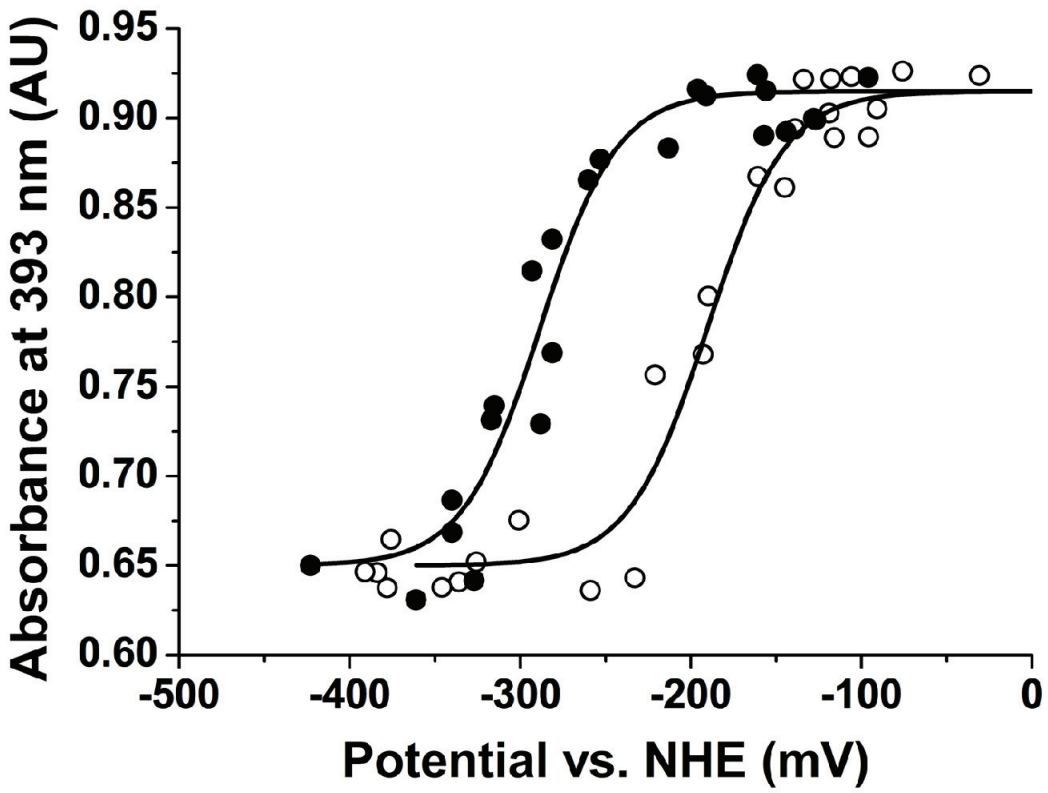
Absorbance at 393 nm (AU)
0.95
0.90
0.85
0.80
0.75
0.70
0.65
0.60
-500
-400
-300
-200
-100
0
Potential vs. NHE (mV)

Figure S4

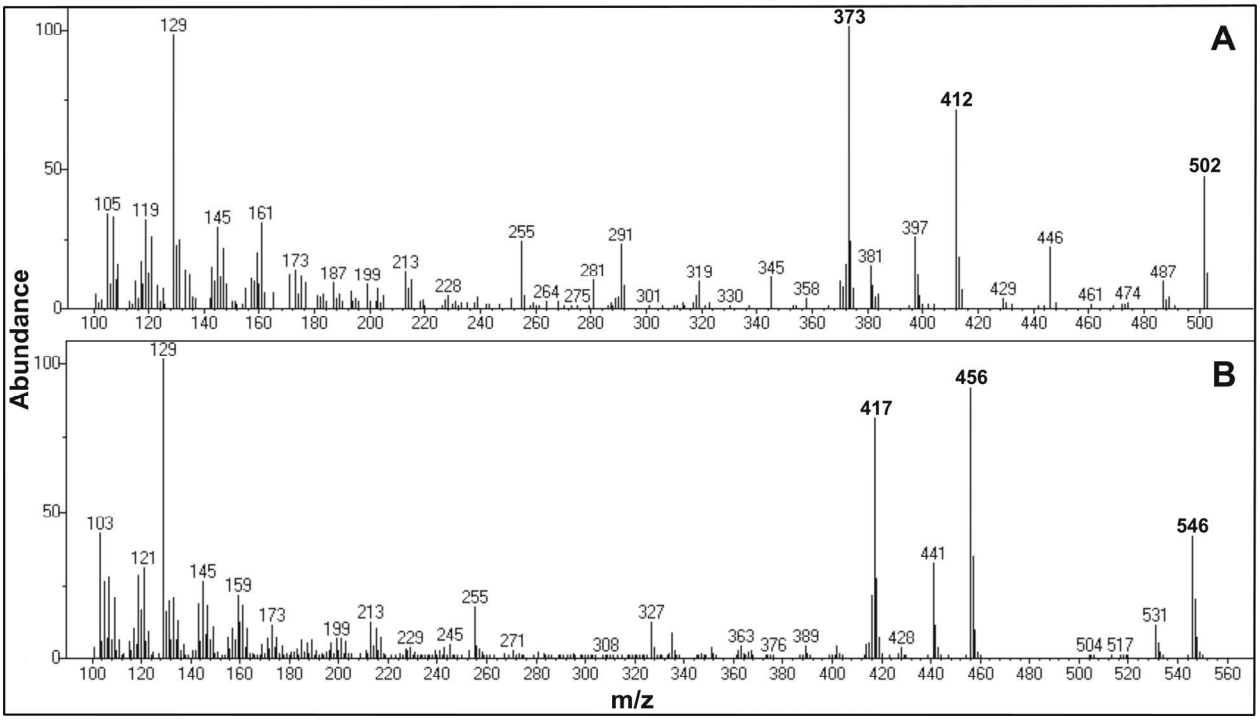
A
B
Abundance
m/z
373
412
502
129
105
119
145
161
173
187
199
213
228
255
264
275
281
291
301
319
330
345
358
381
397
429
446
461
474
487
456
417
546
103
121
159
327
363
376
389
428
441
504
517
531

Figure S5

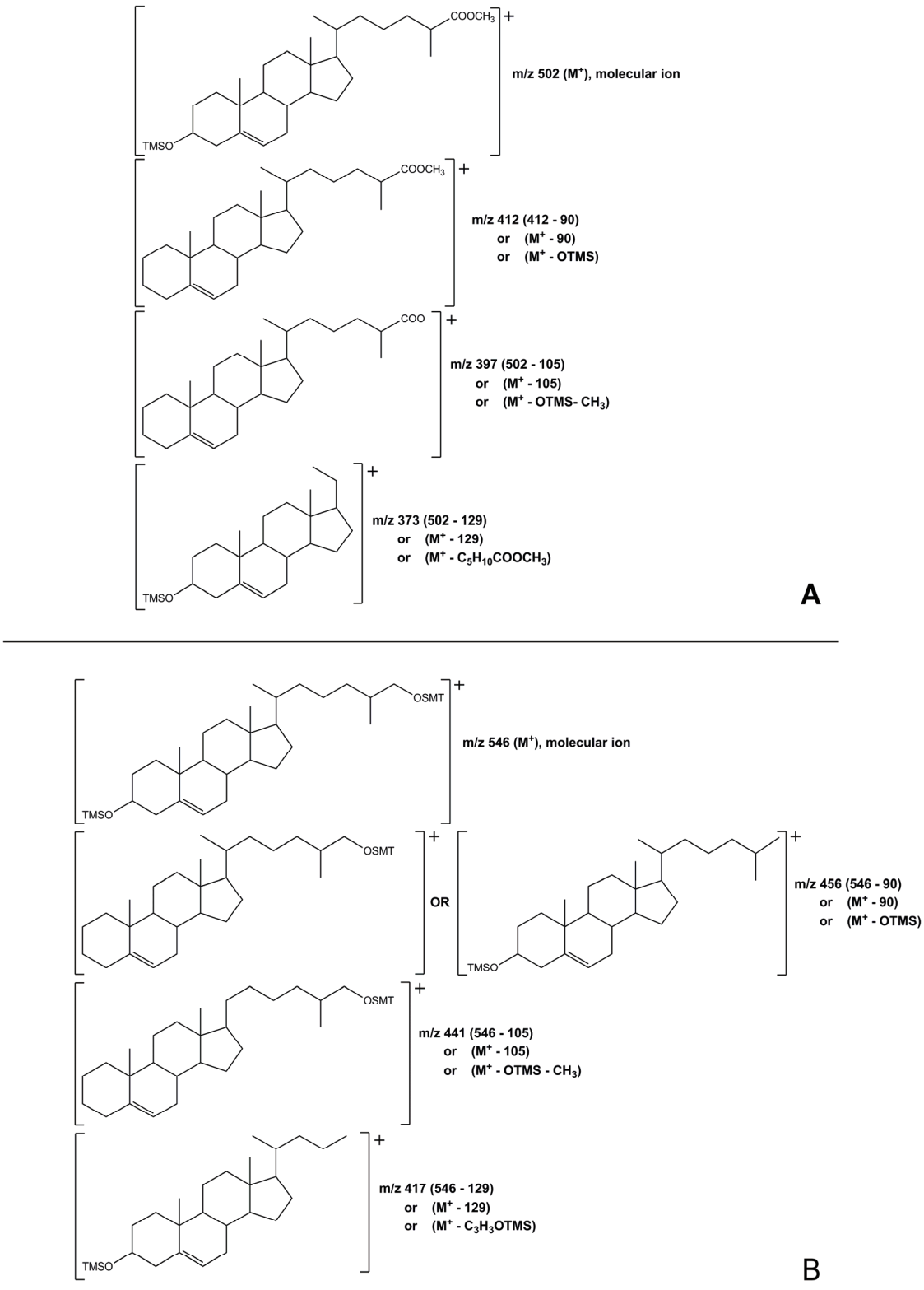
COOCH3
TMSO
m/z 502 (M+), molecular ion
m/z 412 (412 - 90)
or (M+ - 90)
or (M+ - OTMS)
COO
m/z 397 (502 - 105)
or (M+ - 105)
or (M+ - OTMS- CH3)
m/z 373 (502 - 129)
or (M+ - 129)
or (M+ - C5H10COOCH3)
A
OSMT
m/z 546 (M+), molecular ion
OR
m/z 456 (546 - 90)
or (M+ - 90)
or (M+ - OTMS)
m/z 441 (546 - 105)
or (M+ - 105)
or (M+ - OTMS - CH3)
m/z 417 (546 - 129)
or (M+ - 129)
or (M+ - C3H3OTMS)
B

Figure S6

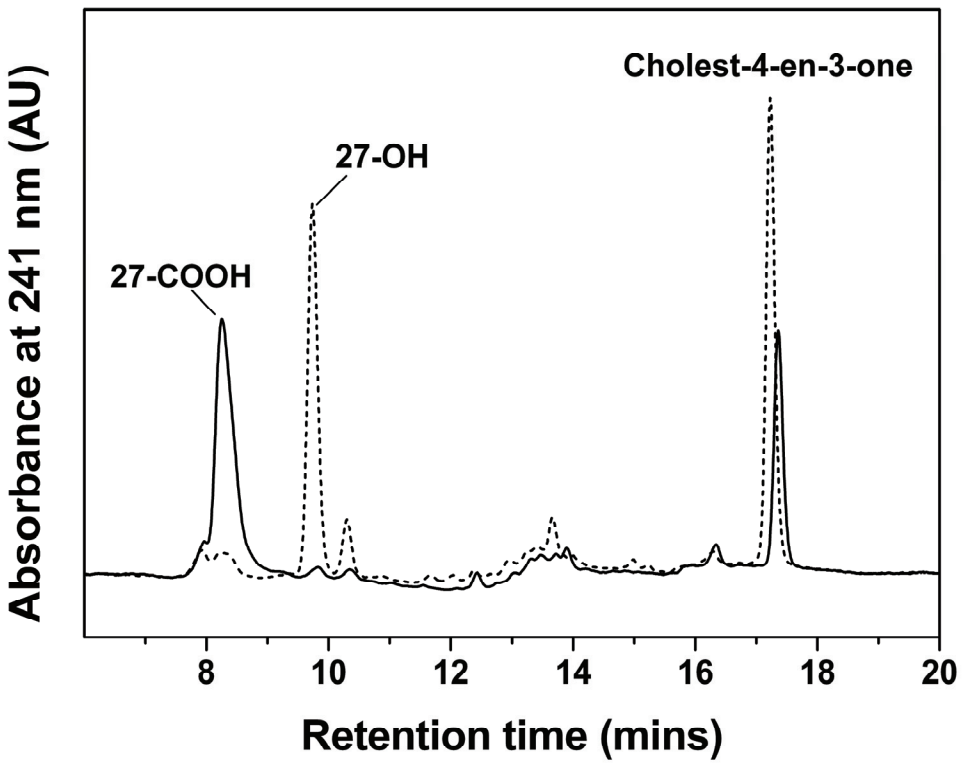
Cholest-4-en-3-one
27-OH
27-COOH
Absorbance at 241 nm (AU)
8
10
12
14
16
18
20
Retention time (mins)

Figure S7

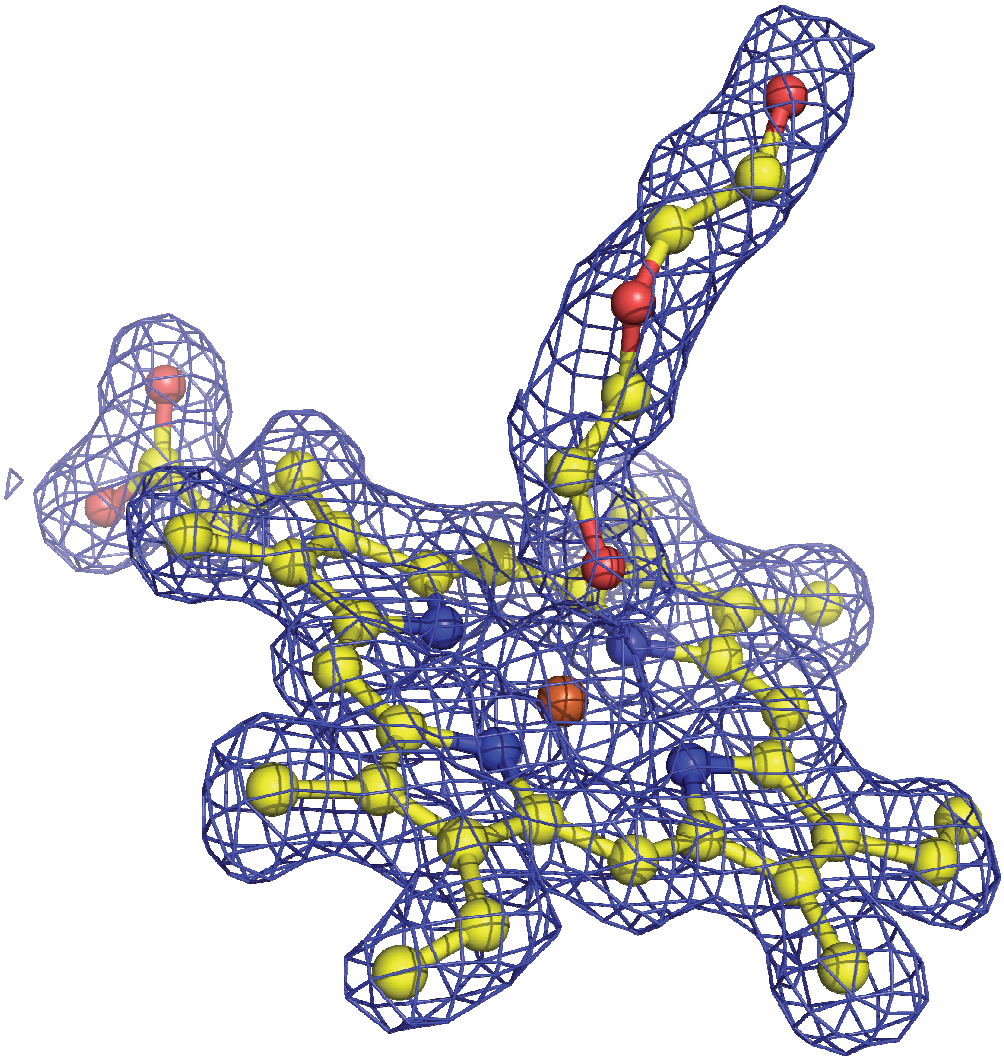

Figure S8

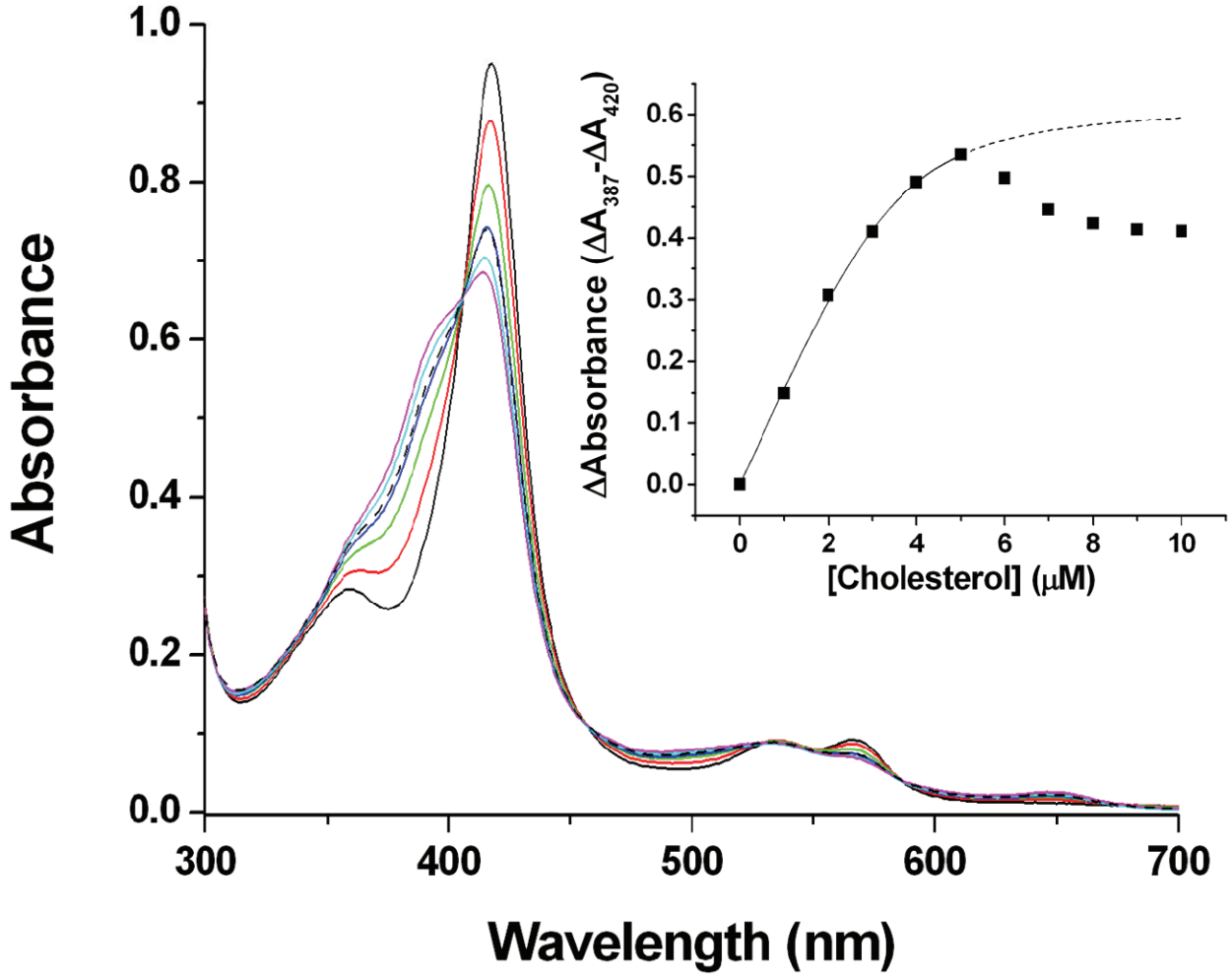
Absorbance
Wavelength (nm)
ΔAbsorbance (ΔA387-ΔA420)
[Cholesterol] (μM)

Figure S9